Solar Energy 207 (2020) 720–728

Contents lists available at ScienceDirect

Solar Energy

journal homepage: www.elsevier.com/locate/solener

A 2,5-difluoro benzene-based low cost and efficient polymer donor for non-fullerene solar cells

Gururaj P. Kini, Hee Seon Park, Sung Jae Jeon, Yong Woon Han, Doo Kyung Moon*

Nano and Information Materials (NIMs) Laboratory, Department of Chemical Engineering, Konkuk University, 120, Neungdong-ro, Gwangjin-gu, Seoul 05029, Republic of Korea

ARTICLE INFO

Keywords:
Non-fullerene solar cells
Scalable polymer donor
Low-cost polymer donor
Fluorine effect
2-5-difluoro benzene

ABSTRACT

Although the latest progress in the power conversion efficiency (PCE) of non-fullerene polymer solar cells (NF-PSCs) has proved their potential as next-generation solar technologies, the development of efficient wide-bandgap (WBG) donor polymers having a low-cost and easily scalable molecular design is still lagging in terms of number and diversity. In this contribution, we report a new WBG polymer donor, PBDT-2FBnT, based on alternative benzodithiophene as the donor unit and 2,5-difluoro benzene (2FBn) as the acceptor unit, which was prepared by a facile three-step process with an overall yield over 80% using cheap raw materials. Benefitting from the incorporation of an electron-deficient 2FBn unit, PBDT-2FBnT demonstrated lower frontier energy levels with an optical bandgap of 2.12 eV. Additionally, the combination of 2FBn with an adjacent two thiophene bridge in the polymer backbone significantly minimized the steric hindrance via non-covalent F···S and C—H···F inter/intramolecular interactions, thereby promoting highly coplanar geometry for effective molecular packing and charge transport. Consequently, optimized blends of PBDT-2FBnT with an ITIC acceptor delivered complementary panchromatic absorption, well-aligned energy levels, higher charge carrier mobilities, and well-distributed nano-fibrillar morphology, thereby leading to a remarkable efficiency of 9.5% with a good trade-off between corresponding photovoltaic parameters. Thus, the high photovoltaic performance of PBDT-2FBnT together with simple preparation can provide a promising way for the future development of low-cost PSCs, and we can foresee further PCE improvements of the PBDT-2FBnT structure via synergistic variation of donor and acceptor material.

1. Introduction

Polymer solar cells (PSCs) are considered to be emerging horizons among the next-generation solar technologies because of their distinctive benefits like lightweight, low cost, semi-transparency, and having the freedom of mechanical flexibility and compatibility with large-scale manufacturing roll-to-roll processes (Berny et al., 2016; Li, Y. et al., 2018; Lu et al., 2015; Ma et al., 2017). In the last four years, the rapid development of non-fullerene PSCs (NF-PSCs) consisting of a wide-bandgap (WBG) polymer donor (PD) and a low-bandgap (LBG) fused-ring small-molecule electron acceptor (FREAs or FR-NFAs) has been witnessed, which delivered accelerated growth in power conversion efficiencies (PCEs) of PSCs (Cui et al., 2019a; Cui et al., 2019c; Hong et al., 2019; Liu, T. et al., 2019; Yuan et al., 2019b; Zhang, S. et al., 2018). This improvement is mainly ascribed to continuous innovation in the rational design of various prominent NFAs series, such as IDTBR-class (Hoefler et al., 2018; Holliday et al., 2016; Strohm et al., 2018), ITIC-type (well-known "ITIC series") (Dey, 2019; Lin et al., 2015; Wadsworth et al., 2019; Yang et al., 2017; Zhao et al., 2017), and fused benzothiadiazole-type ("Y" series) (Cui et al., 2019c; Luo et al., 2019; Yuan et al., 2019a; Yuan et al., 2019b), which simultaneously offer high electron mobilities (μ_e), easy tailoring of absorption, and frontier molecular orbitals via chemical modification for easy charge transport. Among the efficient NFAs reported to date, most of these acceptors use intramolecular charge transfer (ICT) effect as a tool to increase the short-circuit current density (*Jsc*) in corresponding PSCs by incorporating a terminal electron withdrawing unit (Bai et al., 2015; Holliday et al., 2016; Liu, H. et al., 2019) or/and functional group in the molecular design (Dey, 2019; Kini et al., 2020; Li, X. et al., 2017; Li, Y. et al., 2017;Zhao et al., 2017). However, this modification often results in lower open-circuit voltages (*Voc*) in corresponding devices because of the lower lowest unoccupied molecular orbitals (LUMO) levels of NFAs. Thus, increasing *Voc* without sacrificing *Jsc* and FF is one of the key challenges in NF-PSCs. Recently, many reports proved that a WBG-

* Corresponding author.
E-mail address: dkmoon@konkuk.ac.kr (D.K. Moon).

https://doi.org/10.1016/j.solener.2020.06.090
Received 24 May 2020; Received in revised form 22 June 2020; Accepted 24 June 2020
Available online 15 July 2020

PDs:LBG-NFAs blend system can effectively work via a photogenerated hole-transfer mechanism under a lower driving force with a ΔE_{HOMO} (the energy offset among the HOMO of donors (D) and acceptors (A)) < 0.3 eV than that of typical fullerene-based PSCs (Cui et al., 2019c; Li et al., 2021; Wang et al., 2019; Zhang et al., 2019; Zhang, Z. et al., 2017). This development is of great significance, since the pairing of WBG-PDs having deep HOMO could be used as an effective approach for realizing the high *V*oc in the NFAs having very low LUMO levels. Consequently, the design and development of new WBG-PDs with deeper HOMO to better match narrow bandgap FREAs is essential to make a further breakthrough in the PCEs of NF-PSCs.

Among the various "D" building blocks reported to date, two-dimensional (2D)-benzo[1,2-*b*:4,5-*b*′]dithiophene (2D-BDT) seems to be continuously evolved as a prominent "D" unit for synthesizing highly efficient WBG-PDs for NF-PSCs (Pai et al., 2016; Ye et al., 2014). In addition to its fused ring core facilitating the resulting polymers with a highly planar and rigid conjugated backbone thereby increasing charge carrier mobility via effective charge delocalization along the polymer backbone, they also enable easy tuning of energy levels and solubility by varying the alkyl side chain on the BDT unit (Pai et al., 2016; Ye et al., 2014). Moreover, its weak electron-donating nature also aids in achieving higher *V*oc in PSCs by efficiently lowering the HOMO. Subsequently, a variety of efficient WBG-PDs have been synthesized by incorporating BDT as "D" unit and various "A" units, such thieno[3,4-*c*] pyrrole-4,6-dione (Hadmojo et al., 2019; Lin et al., 2017), quinoxaline (Li, L. et al., 2018; Xu et al., 2018), benzotriazole (Liao et al., 2019; Su et al., 2019) and benzo [1,2-*c*:4,5-*c*']dithiophene-4,8-dione (BDD) (Cui et al., 2019b; Liu, T. et al., 2019; Yuan et al., 2019b), which have demonstrated excellent photovoltaic performances. Despite such remarkable improvements of PCEs of these BDT-based WBG-PDs, the high cost and tedious synthesis involved in the preparation of these photovoltaic materials is causing major hurdles for the commercialization of PSCs. To address this issue, recently a few groups developed an easily scalable polymer design involving alternate BDT and thiophene and/or heteroarene units with various electron-withdrawing substituents as a weak "A" unit owing to their advantages of low cost, simple and straightforward synthesis involving fewer steps, high scalability, and superior stability (Fig. 1) (Firdaus et al., 2017; Jeon et al., 2019a; Kini et al., 2019; Park et al., 2017).

For example, Beaujuge and co-workers reported a new 2D-BDT-based copolymer, PBDT(T)[2F]T, using 2,5-dibromo-3,4-difluoro-thiophene (2FTh) as the "A" core, which was synthesized in an easy three-step process (Firdaus et al., 2017). Because of the insertion of 2FTh, the polymer demonstrated deep HOMO, also excellent charge-generation/collection efficiencies with minimized germinate recombination in NF-PSCs yielding the best PCE of 9.8% with a significant improvement in *V*oc up to 0.94 V. In another instance, Chen et al. obtained WBG-PD ca. 3MT-Th based on 2D-BDT-alt methyl 2,5-dibromothiophene-3-carboxylate, which was prepared using a simple, straightforward two steps (Park et al., 2017). The corresponding NF-PSCs processed using the non-halogen solvent toluene with 0.25% diphenyl ether demonstrated a notable PCE of 9.73% with excellent stability under continuous illumination. Further, Jeon et al. also recently achieved a remarkable PCE of 12.14% and excellent long-term stability with the easily scalable polymer design involving alternate BDT and 2,5-dibromo-3-chloro thiophene (Jeon et al., 2019a). By adopting a similar approach, in our previous research, we also synthesized polymer BDT-PYEH consisting of BDT and pyrazine as "D" and "A" units, respectively which displayed a notable PCE of 8.1% (Kini et al., 2019). The increase in the performance was attributed to the incorporation of an electron-deficient pyrazine unit in the polymer backbone, which conferred deep-lying HOMO, increased coplanarity, efficient charge dissociation, and optimal nanoscale morphology. As a result, the molecular design strategies involving BDT and heteroacene are believed to be a more reliable approach for producing efficient WBG-PDs with tunable energy levels and lower synthetic complexity, thereby offering meaningful direction towards scalable PSCs.

Motivated by the aforementioned research, here we propose a new low-cost 2D-BDT-based WBG-PD, poly-{2-(3-(2-ethylhexyl)-5-(4-(4-(2-ethylhexyl)-5-methylthiophen-2-yl)-2,5-difluorophenyl)thiophen-2-yl)-4,8-bis(5-(2-ethylhexyl)thiophen-2-yl)-6-methylbenzo[1,2-*b*:4,5-*b*']dithiophene} (PBDT-2FBnT) prepared by introducing an electron deficient "2,5-difluoro benzene (2FBn)" unit as the "A" core (Fig. 1). Among a very few easily accessible electron-deficient heteroacene units, "2FBn" was selected considering its various advantageous properties as follows: (a) The drafting of 2FBn can provide polymer semiconductors with lower HOMO and subsequently higher *V*oc because of the large aromatic resonance energy of the phenylene moiety and strong electronegativity of the fluorine (F) atom (Chen et al., 2017; Yang et al., 2018; Zhang, Q. et al., 2017). (b) The smaller atomic radii of the F atom will effectively minimize the undesirable steric repulsion as observed in other electron-deficient units, such as chlorine, cyano, and carboxylate, thereby increasing the coplanarity of the polymer backbone (Li, S. et al., 2018; Zhang, Q. et al., 2017; Zhang, Y. et al., 2018). (c) The symmetrically placed F-substituents (C2 symmetry) can induce self-planarization of the conjugated backbone via formation of non-covalent F···S, C−H···F, etc., coulombic interactions with adjacent thiophene units, subsequently leading to an increased absorption coefficient and overall charge carrier mobilities by improving molecular crystallinity and aggregation (Chen et al., 2017; Yang et al., 2018). (d) Relative to other fluorinated intermediates involving higher production cost because of tedious synthetic steps and poor yield, the 2FBn unit is commercially available at a lower cost and is therefore advantageous for large-scale production. Thus, we systematically evaluated the influence of a 2FBn unit on the optoelectronic and photovoltaic performances of PBDT-2FBnT by using various characterization methods. As expected, with the benefits from the insertion of the 2FBn unit, PBDT-2FBnT showed a deep HOMO level of −5.48 eV without negatively affecting the optical bandgap (ca. 2.12 eV), and therefore a superior *V*oc of 0.919 V was achieved from the optimized NF-PSCs with an ITIC acceptor. Moreover, resulting from the stronger molecular aggregations, face-on molecular orientation, high carrier mobilities, and the superior BHJ morphology of the PBDT-2FBnT:ITIC blend, a high *J*sc (16.1 mA/cm^2), FF (64.1%), and an outstanding PCE of 9.5% were also achieved. These outcomes reveal that the inexpensive 2FBn building block can be effectively used as a weak electron-accepting core for designing WBG-PDs, and PBDT-2FBnT has promising potentials in NF-PSCs.

2. Results and discussion

The detailed synthetic path of the monomer and polymer is presented In Fig. 2a and b. The intermediate tributyl(4-(2-ethylhexyl) thiophen-2-yl)stannane (**2**) was prepared following the previously stated procedure (Biniek et al., 2010). Then, the desired 5,5′-(2,5-difluoro-1,4-phenylene)bis(2-bromo-3-(2-ethylhexyl)thiophene) (**M1**) monomer unit was prepared by a simple two-step process. First, the compound 5,5′-(2,5-difluoro-1,4-phenylene)bis(3-(2-ethylhexyl)thiophene) (**3**) was obtained by a Stille coupling reaction between commercially available low-cost 1,4-dibromo-2,5-difluorobenzene (**1**) and compound **2** using $Pd(PPh_3)_4$ with a yield of 82%. Then, subsequent functionalization of compound **3** using *N*-bromosuccinimide was carried out to afford the final target monomer **M1** with an 84% yield. Finally, the target polymer PBDT-2FBnT was synthesized via a microwave-assisted Stille polymerization between monomers **M1** and **M2** in chlorobenzene (CB) with a yield of over 88%. The detailed procedures, including the characterization data, are provided in the Experimental section of the ESI. As prepared PBDT-2FBnT was easily processed using common organic solvents such as chloroform (CF), CB, and o-dichlorobenzene. PBDT-2FBnT showed a number-averaged molecular weight (M_n)/ polydispersity index (PDI) of 75.49/2.10, which was analyzed by gel-permeation chromatography (GPC) against polystyrene

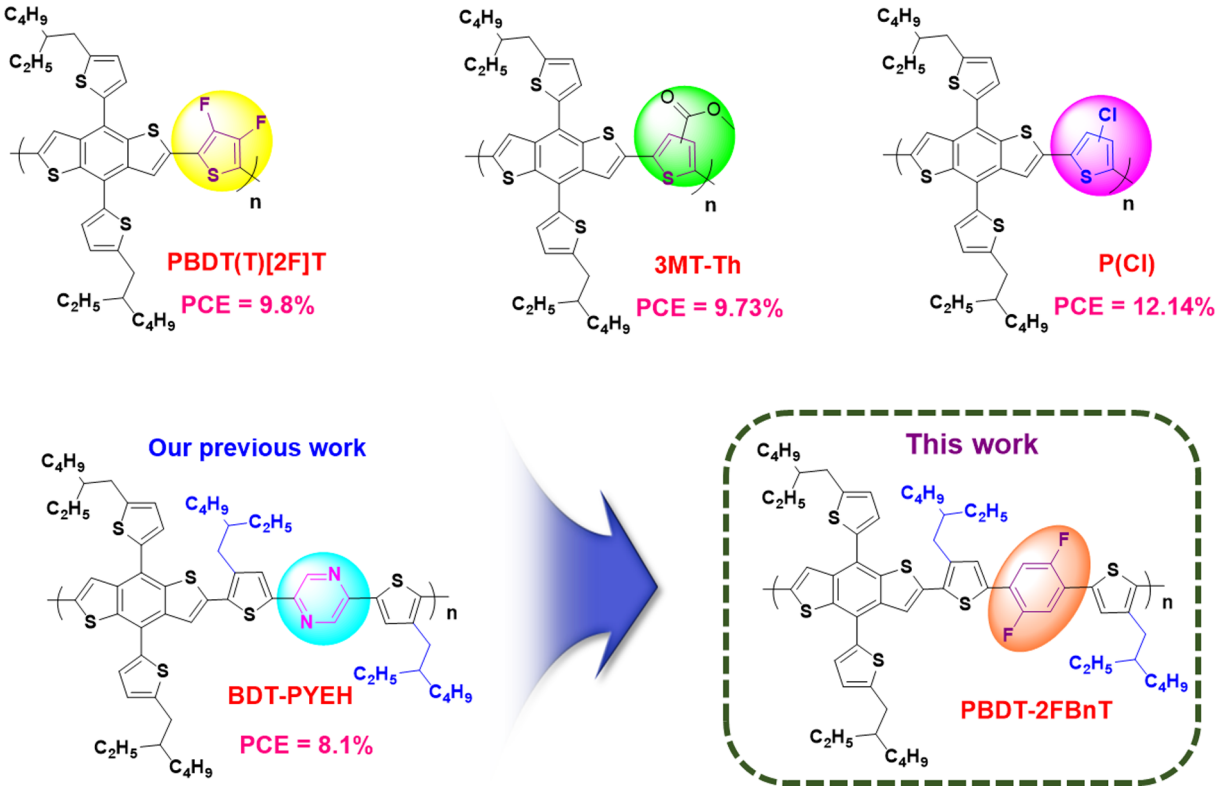

Fig. 1. Chemical structures of the representative easily scalable WBG-PDs based on a "BDT-alt-heteroacene" molecular structure and structure of the new BDT-2FBnT reported in this work.

standards. Meanwhile, there was no noticeable change seen in the thermogravimetric analysis (TGA) profiles of PBDT-2FBnT until temperature exceeding 330 °C, which is sufficient for PSCs application (Fig. S1).

To foresee the influence of 2FBn on the geometry and electronic structures of PBDT-2FBnT, we conducted density functional theory (DFT) computations using Gaussian 09 program at B3LYP/6-31G(d) basic set. To save time and simplify the calculation, we did simulations based on the two-repeating unit of PBDT-2FBnT (Fig. 2c). Notably, the optimal dihedral angle between 2FBn and its adjacent thiophene units (1.15° and 0.9°) was substantially smaller than between BDT units (31.86° and 35.02°). This indicated that F substituents on 2FBn unit increased backbone planarity by diminishing undesirable steric hindrance in the polymer backbone by forming the non-covalent S···F and S···H conformational locks with the adjacent thiophene units as reported previously (Chen et al., 2017; Yang et al., 2018). Moreover, it can be seen from the side view that the backbone of the PBDT-2FBnT exhibits a highly coplanar structure, which is helpful for effective molecular packing and charge transport. The HOMO and LUMO energy levels of the PBDT-2FBnT, as calculated from the DFT simulations, were −4.88 and −2.13 eV, respectively, and variation of these trends was comparable with experimental cyclic voltammetry (CV) values as discussed below.

The normalized UV–vis spectra of copolymer PBDT-2FBnT in CF solution and the thin film state is shown in Fig. 3a, and the relative optical parameters are outlined in Table 1. In both states, PBDT-2FBnT showed a characteristic dual-band absorption profile between 300 and 570 nm, which is complementary to 3,9-bis(2-methylene-(3-(1,1-dicyanomethylene)-indanone))-5,5,11,11-tetrakis(4-hexylphenyl)-dithieno[2,3-*d*:2′,3′-*d*′]-*s*-indaceno[1,2-*b*:5,6-*b*′]dithiophene (ITIC) acceptor, so blending of both components can facilitate effective harvesting of the solar spectrum by covering a panchromatic absorption. The first weak absorption band around 300–400 nm originates from the localized π–π* transitions; whereas the next intense band at 450–600 nm is assigned to ICT from a BDT to 2FBn unit in the polymer backbone (Kini et al., 2018; Kini et al., 2017a). The molar absorptivity coefficient (ε) of PBDT-2FBnT found to be 5.39 × 10^4 M^{-1} cm^{-1} (Fig. S2), which will definitely aid the increase of photoelectric current in the PSC devices. In relative to the absorption in the solution state, the absorption profile of PBDT-2FBnT in the film state not only showed large red-shifted absorption (~50 nm), but also demonstrated a much broader spectrum with a distinct vibrionic peak at ca. 570 nm. Such transition of spectra suggested the strong intermolecular stacking between the polymer chains, which could originate from noncovalent interactions of the F atom. The optical bandgap of PBDT-2FBnT is calculated to be 2.12 eV from the absorption onset of polymer in the film state.

By using CV, we evaluated the electrochemical properties of the PBDT-2FBnT. As depicted in Fig. 3b, onset oxidation/reduction potential of PBDT-2FBnT was 1.14/-0.89 eV *vs.* saturated calomel electrode (Ag/Ag^+). So, by using equation $E_{HOMO\ (or\ LUMO)} = -[E_{onset}(vs\ Ag/AgCl) - E_{1/2}\ of\ Fc/Fc^+(vs\ Ag/AgCl)] - 4.8$ [eV] (Measured $E_{1/2}$ of Fc/Fc+ (*vs.* Ag/AgCl) = 0.46 eV) corresponding HOMO/LUMO were estimated to be −5.48/−3.45 eV, respectively. As predicted, the presence of the phenylene moiety with two electrophilic F substituents aided in lowering both frontier molecular orbitals of PBDT-2FBnT, which will certainly help to realize high *Voc* in the PSCs. Besides, it can be clearly seen in Fig. 3c that a clear cascade energy level alignment is formed between the PBDT-2FBnT and ITIC acceptor with a small HOMO energy offset ($\triangle E_{HOMO}$) = 0.07 eV < 0.3 eV, which can be advantageous for efficient exciton dissociation and charge transfer as observed in several recent high-efficiency NF-PSCs (Cui et al., 2019c; Wang et al., 2019; Zhang et al., 2019; Zhang, Z. et al., 2017).

To evaluate the potential of PBDT-2FBnT as a "D" unit, we fabricated the inverted PSCs devices with a structure of ITO/ZnO/active layer/MoO_3/Ag (Jeon et al., 2019b). At first, PSCs device condition was systematically optimized by changing the blend ratio of PBDT-2FBnT and ITIC and processing solvents. We found that the device with the

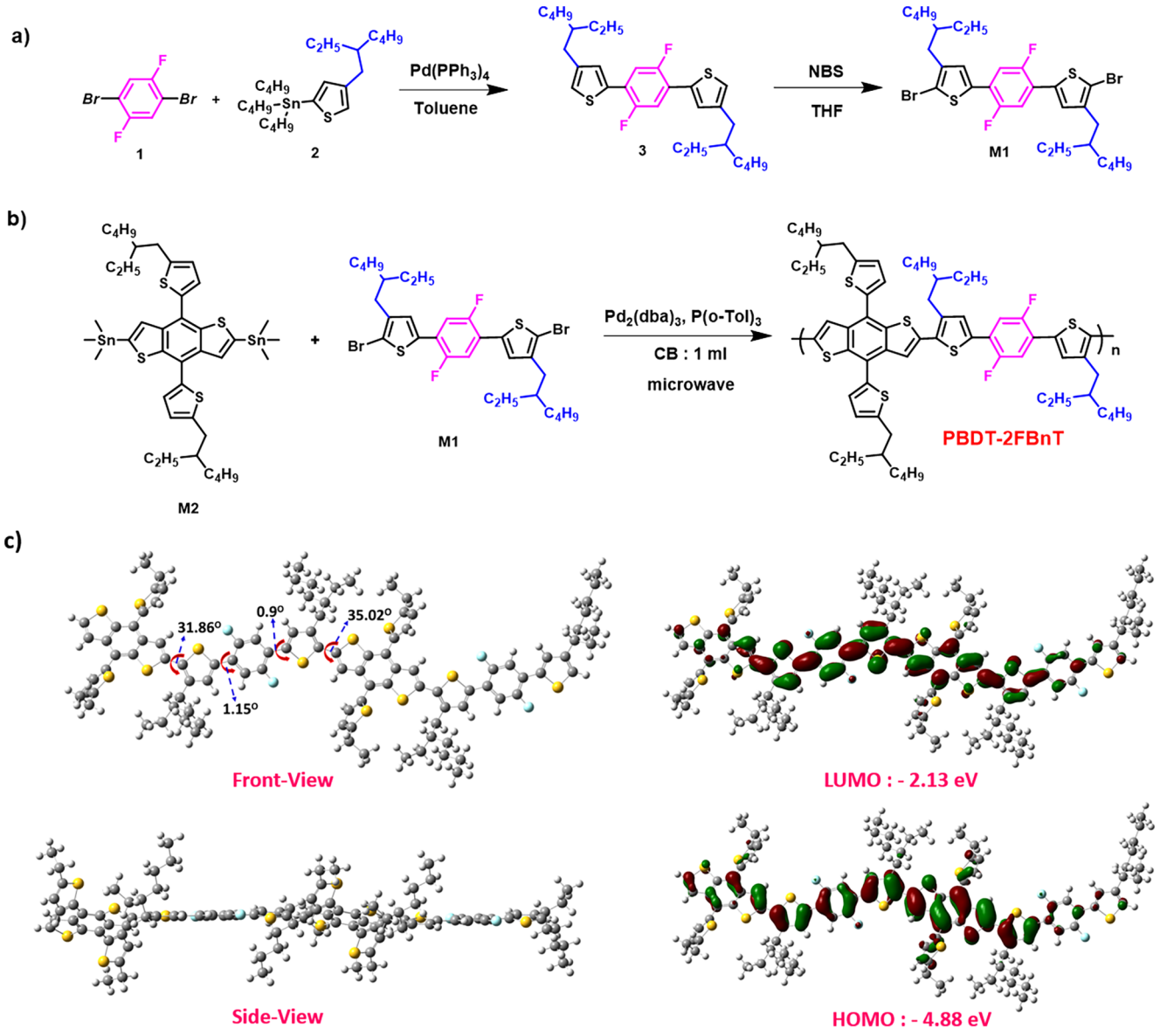

Fig. 2. Synthetic routes of (a) monomer, (b) polymer BDT-2FBnT and (c) optimized molecular geometries and frontier molecular orbitals of BDT-2FBnT dimers.

1:1 wt ratio of PBDT-2FBnT:ITIC, processed using CB and a thermal annealing temperature of 110 °C for 10 min afforded the best PCE of 7.2% with corresponding *Voc* of 0.899 V, *Jsc* of 15.5 mA/cm^2, and FF of 51.7% (Fig. S3 and Table S1). Later, considering the fact that methods like thermal annealing and/or solvent additives are used to increase the efficiency of NF-PSCs by optimizing the nanoscale morphology and crystalline phases of the blend films (Gao et al., 2018; Song et al., 2018; Wienhold et al., 2019), we exploited these proven methods to further boost the efficiency in our system. Fig. 4(a) represents the current density-voltage (*J-V*) curves of the optimal PSCs based on PBDT-

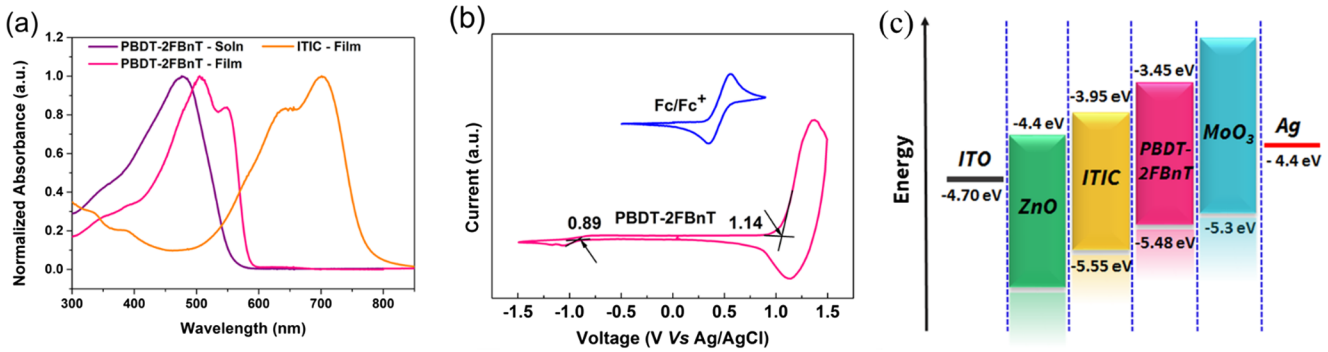

Fig. 3. Normalized absorption spectra of PBDT-2FBnT in (a) a chloroform solution and the thin-film state, (b) cyclic voltammograms and (c) energy level alignment for PBDT-2FBnT and ITIC.

Table 1
Summary of thermal, optical, and electrochemical properties of the PBDT-2FBnT polymer.

Polymer	M_n [kDa]/ PDI[a]	Thermal property	Optical properties					Electrochemical properties	
		T_d [°C][b]	λ_{max} [nm], solution	ε (10^4) [M^{-1} cm^{-1}][c]	λ_{max} [nm], thin film	λ_{onset} [nm], thin film	E_g^{opt} [eV][d]	HOMO [eV]	LUMO [eV]
PBDT-2FBnT	75.49/2.10	352	476	5.39	505, 550	585	2.12	−5.48	−3.45

[a] Measured by GPC.
[b] Decomposition temperature (Td, with 5% weight loss) was calculated by TGA.
[c] The molar extinction coefficient of polymers at 475 nm in CF solution was measured using the Beer-Lambert law ($A = \varepsilon bc$).
[d] Estimated values from the UV–vis absorption edge of the thin film ($E_g^{opt} = 1240/\lambda_{onset}$, eV).

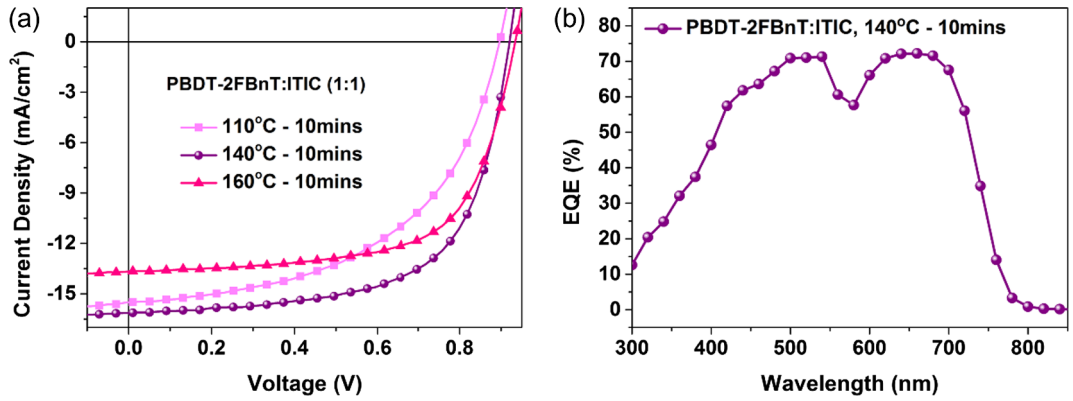

Fig. 4. (a) The *J-V* curves of optimal PSCs based on PBDT-2FBnT:ITIC devices processed with different thermal annealing temperatures and (b) corresponding EQE spectra of the optimal devices.

Table 2
The photovoltaic parameters of the optimized PSCs based on PBDT-2FBnT:ITIC (1:1) devices processed with different thermal annealing temperatures under AM 1.5G illumination at 100 mW cm^{-2}.

Blend	Annealing temperature [°C]	V_{OC} [V][a]	J_{SC} [mA cm^{-2}][a]	FF [%] [a]	PCE[a] [%]	μ_h [cm^2 V^{-1} s^{-1}][b]	μ_e [cm^2 V^{-1} s^{-1}][c]	μ_h/μ_e
PBDT-2FBnT: ITIC (1:1)	110	0.899 (0.899 ± 0)	15.5 (15.45 ± 0.5)	51.7 (50.8 ± 0.9)	7.2 (6.95)	1.33×10^{-4}		
	140	0.919 (0.919 ± 0)	16.1 (15.8 ± 0.3)	64.1 (62.9 ± 1.2)	9.5 (9.25)		1.07×10^{-4}	1.24
	160	0.939 (0.92 ± 0.02)	13.7 (13.3 ± 0.4)	64.9 (62.4 ± 2.5)	8.3 (7.9)			

Device architecture: ITO/ZnO/active layer/MoO_3/Ag.
[a] The average values and standard deviations were derived from 6 to 8 independent devices.
[b] The hole-only device had the configuration ITO/PEDOT:PSS/active layer/MoO_3/Ag.
[c] The electron-only device had the configuration ITO/ZnO/active-layer/LiF/Al.

2FBnT:ITIC (1:1) blend with different thermal annealing temperatures (110, 140, and 160 °C) under AM 1.5G illumination, and subsequent parameters are arranged in Table 2.

Noticeably, as the thermal annealing temperature was increased from 110 °C to 140 °C, the PCEs of PBDT-2FBnT based devices were significantly improved; however, at 160 °C yet again drop in the PCEs was observed. Fascinatingly, thermally annealed optimal PBDT-2FBnT:ITIC blend films at 140 °C for 10 min afforded the highest PCE of 9.5% with resultant photovoltaic parameters *V*oc = 0.919 V, *J*sc of 16.1 mA/cm^2 and FF of 64.1%. The larger *V*oc and remarkably high *J*sc result from the lower HOMO and stronger interchain interactions in the solid-state, respectively, and are mainly attributed to the insertion of 2FBn in the polymer backbone. Meanwhile, these devices also demonstrated a significantly improved FF from 51.7% at 110 °C to 64.1% at 140 °C, emphasizing that thermal annealing enabled an intrinsically favorable phase-separated BHJ morphology promoting efficient charge transport. However, further increase of the thermal annealing temperature from 140 °C to 160 °C hampered the optimal trade-off between the *J*sc and *V*oc observed in the best devices; so, these devices demonstrated a marginally lower PCE of 8.3%. Besides, we also tested the effect of a different high-boiling solvent additive such as 1, 8-diiodooctane (DIO) and 1-chloronaphthalene (CN) along with thermal annealing. Although these devices showed maximum PCEs up to 9.2%, there was no further improvement in the PCEs observed when compared to devices without a solvent additive (Fig. S4-5 and Table S2-3). External quantum efficiency (EQE) profiles of champion PBDT-2FBnT:ITIC devices are displayed in Fig. 4b. The integrated *J*sc value achieved from the EQE curve was 14.27 mA/cm^2, which is consistent with the *J*sc value of 16.1 mA/cm^2 obtained in the *J–V* measurement with reasonable mismatch range. Thus, owing to the effective contributions of both PBDT-2FBnT and ITIC, optimal PSCs exhibited higher EQE values along the 300–700 nm region and a peak EQE value reaching ~70% at ca. 640 nm, resulting in a remarkable photocurrent in PSCs.

To get a greater understanding of the superior *J*sc, first, we evaluated charge dissociation characteristics of the blend film using the photoluminescence (PL) quenching method. As shown in Fig. 5a, pristine PBDT-2FBnT displayed a pronounced PL emission spectrum located at 580–900 nm with a main peak centered around 715 nm by an exciting film at 550 nm. But, after blending with ITIC, the emission profile

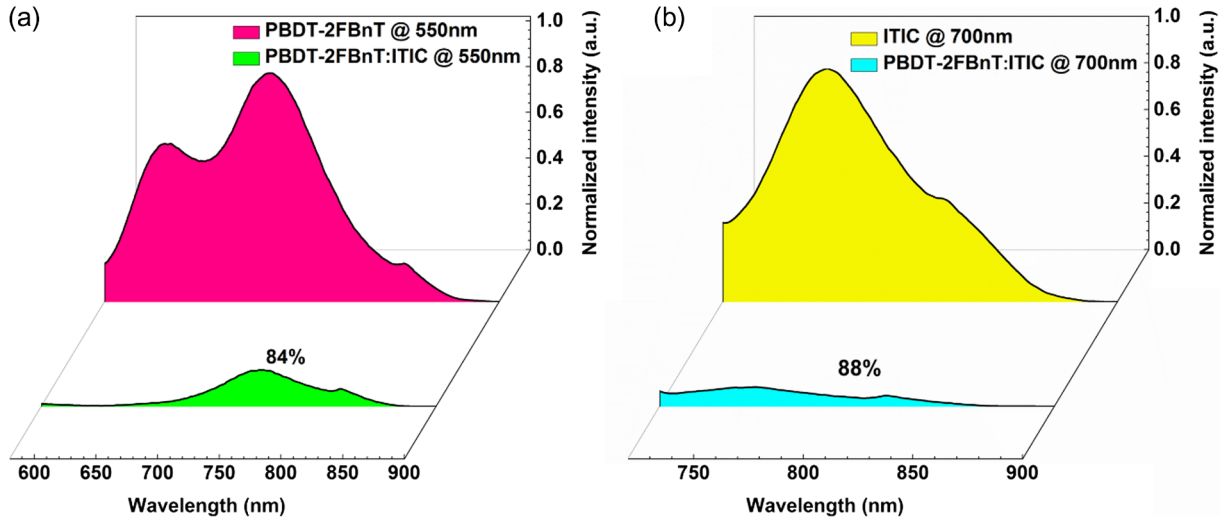

Fig. 5. The photoluminescence spectra of PBDT-2FBnT (excited at 550 nm), ITIC (excited at 700 nm), and optimal PBDT-2FBnT:ITIC blend films (1:1) (excited at 550 and 700 nm).

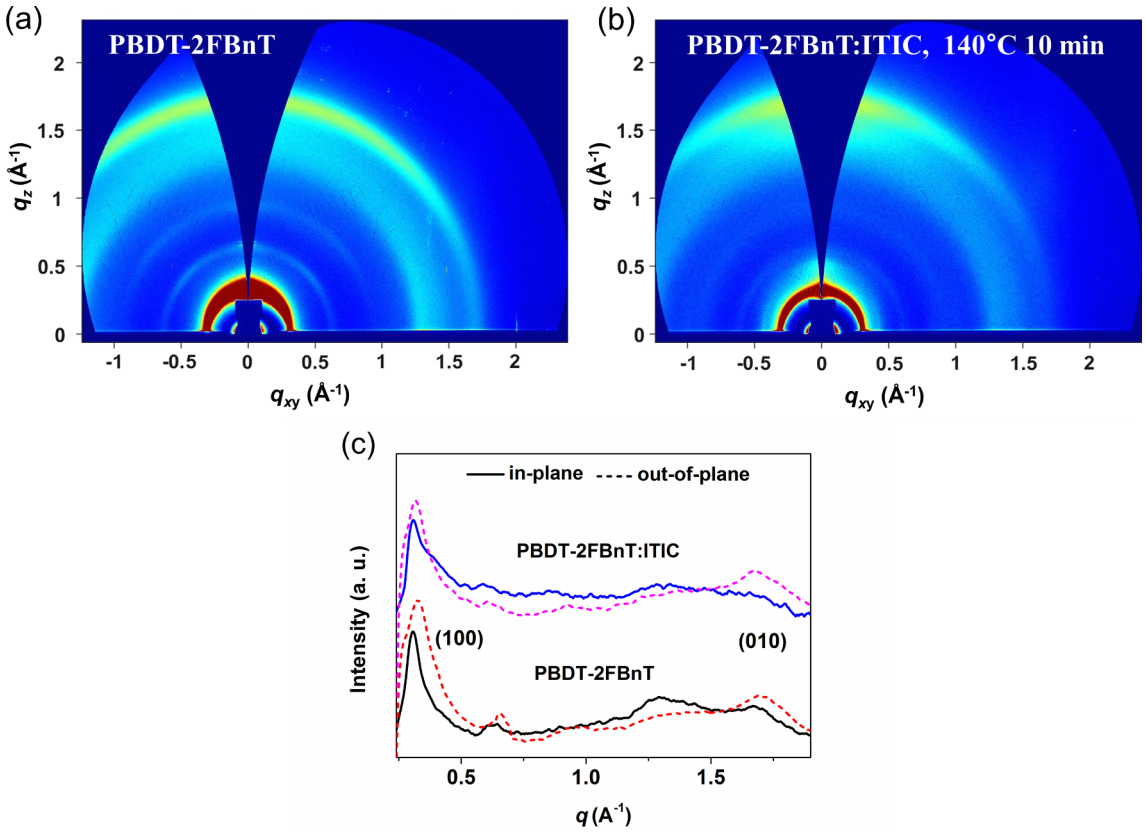

Fig. 6. 2D-GIWAXS images of (a) pure PBDT-2FBnT, (b) optimal PBDT-2FBnT:ITIC blend, and (c) the corresponding out-of-plane and in-plane line cut profiles of the GIWAXS images.

of the optimal blend film was quenched by almost 84%. This implying exciton generated in the PBDT-2FBnT effectively dissociated into the ITIC via photoinduced electron transfer (Kini et al., 2018, 2019; Yang et al., 2018). Similarly, to evaluate the hole transfer efficiency from ITIC to polymer, both ITIC and optimal-blend films were excited at 700 nm (Fig. 5b). Notably, compared to pristine ITIC, the PL emission spectra of blend film was quenched by 88%, suggesting that the extent of hole transfer is also like that of electron transfer. These PL results will further substantiate that photogenerated excitons are effectively dissociated even at a small HOMO energy offset ($\triangle E_{HOMO}$) of 0.07 eV. Thus, a relatively deep HOMO of PBDT-2FBnT and efficient dissociation of photoinduced excitons in the blend films contribute to simultaneously increasing the *J*sc and *V*oc in the optimal PSCs.

To correlate the effect of molecular ordering, crystallinity, and bulk morphology with the photovoltaic performance, we analyzed the two-dimensional grazing incidence wide-angle X-ray scattering (2D-GIWAXS) of pristine PBDT-2FBnT as well as its optimal blend films. The GIWAXS images and the related line-cut profiles are illustrated in Fig. 6, and Table 3 summarizes the resulting packing parameters extracted from these images. The pristine PBDT-2FBnT film demonstrated intense

Table 3
GIWAXS packing parameters of pure PBDT-2FBnT and optimal PBDT-2FBnT:ITIC blend.

Film	IP[a]		OOP[b]	
	d-(1 0 0) [Å]/ (q-(1 0 0) [Å^{-1}])	d-(0 1 0) [Å] / (q-(0 1 0) [Å^{-1}])	d-(1 0 0) [Å]/ (q-(1 0 0) [Å^{-1}])	d-(0 1 0) [Å]/ (q-(0 1 0) [Å^{-1}])
PBDT-Bn2F	20.39 (0.308)	3.76 (1.67)	19.26 (0.326)	3.76 (1.67)
PBDT-Bn2F:ITIC	20.52 (0.306)		19.81 (0.317)	3.74 (1.68)

[a] Calculation from [a]*xy*-axis and [b]z-axis, respectively.

(1 0 0) Braggs reflection peaks along both in-plane (IP) and out-of-plane directions (OOP) (at 0.308 Å^{-1}/0.326 Å^{-1}, respectively), which corresponds to lamellar stacking distances of approximately 20.39 and 19.26 Å, respectively (Fig. 6a and c).

Additionally, they also showed pronounced arc-shaped (0 1 0) π-π stacking peak at 1.67 Å^{-1} along both directions (corresponding d-spacing distance is ~ 3.76 Å), suggesting that neat films of PBDT-2FBnT tend to form typical "bimodal" (i.e. the mixture of "edge-on" and "face-on") molecular orientation. Thus, higher crystallinity of PBDT-2FBnT, which might be ascribed to the introduction of a 2FBn unit in the molecular design, which simultaneously favors a more organized planar backbone and stronger interchain π-π stacking, as evidenced by UV–vis spectra and DFT calculation. After mixing with ITIC, though PBDT-2FBnT:ITIC blend film demonstrated well-resolved (1 0 0) scattering peaks in both directions with nearly similar lamellar spacing (d_{100} IP/OOP = 20.52/19.81 Å, respectively), they exhibited π-π stacking diffraction peak only along the OOP direction (Fig. 6b and c). These results clearly emphasize the change of molecular orientation that occurred from mixed in the case of pure PBDT-2FBnT films to typical "face-on" in the blend films, which is advantageous for vertical charge transport in PCSs (Kini et al., 2016; Li, S. et al., 2018; Wu et al., 2019; Yang et al., 2018). Moreover, these blend films also demonstrated a substantially increased and sharper (0 1 0) diffraction peak along the OOP direction together with a lower π-π stacking distance than that of pure PBDT-2FBnT (~3.74 Å *vs.* ~ 3.76 Å), emphasizing that the crystallinities and molecular ordering of the blend components were substantially increased. Consequently, improved molecular ordering along with "face-on" molecular arrangements of blend film certainly aided efficient charge transport in PSCs, which in turn was reflected in superior *Jsc*, FF, and improved PCEs.

The space-charge-limited current (SCLC) measurement technique was utilized to reveal the effect of charge carrier mobilities on the remarkable PCEs of the optimized PBDT-2FBnT:ITIC blend film. The hole (μ_h) mobilities and μ_e were calculated by fabricating hole-only (ITO/PEDOT:PSS/active-layer/MoO_3/Ag) and electron-only (ITO/ZnO/active-layer/LiF/Al) devices under optimum conditions. Fig. 7a and b represents the resulting dark *J-V* characteristics of the corresponding devices. The optimal blend showed a significantly high μ_h and μ_e of 1.33×10^{-4} and 1.07×10^{-4} cm^2 V^{-1} s^{-1}, respectively, with a μ_h/μ_e ratio of 1.24. As revealed in GIWAXS analysis, these higher charge-carrier mobilities were consistent with stronger intermolecular packing and predominant "face-on" molecular orientation exhibited by optimal PBDT-2FBnT:ITIC blends, which will be useful to minimize the charge recombination (Kini et al., 2017b). Moreover, a good charge balance between μ_h/μ_e will further boost the efficient collection of charges at the respective electrodes by decreasing the charge accumulation (Sharma et al., 2020; Wang et al., 2019). Consequently, high and balanced charge-carrier mobilities were the reason behind higher FF and *Jsc* in the optimal devices.

Finally, we used atomic force microscopy (AFM) and transmission electron microscopy (TEM) to better understand the correlation between surface and bulk morphology of the active layer with photovoltaic performances. As revealed from the AFM phage and height images (Fig. 7c and d), optimal PBDT-2FBnT:ITIC showed rather

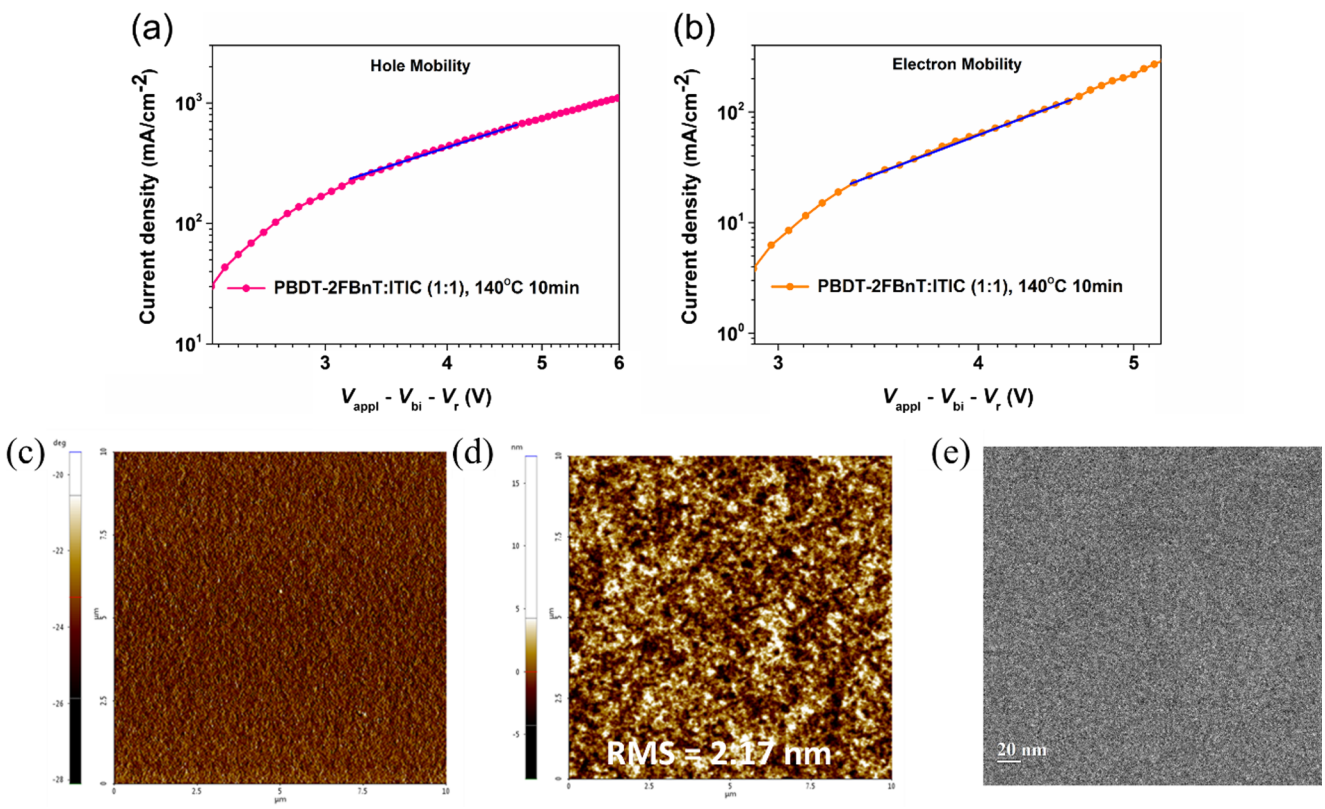

Fig. 7. *J-V* characteristics of (a) hole-only and (b) electron-only devices, (c) AFM phase image, (d) AFM height image and (e) TEM images of the optimal PBDT-2FBnT:ITIC blend film.

uniform and smooth surfaces accompanied by the small relative root mean square roughness (RMS) of 2.17 nm. Moreover, no obvious phase separation was observed, suggesting good intermixing of distinct polymer and ITIC phases. Furthermore, the distinctive nanoscale morphology together with the formation of a bicontinuous interpenetrating network was also clearly distinguishable in the TEM images of this blend (Fig. 7e), which certainly facilitated effective charge carrier dissociation and transport in PSCs. Consequently, it is plausible that higher FF, *J*sc, and photovoltaic performances of PBDT-2FBnT:ITIC devices can be ascribed to several favorable properties, such as optimal morphology, face-on molecular orientation, effective charge dissociation, higher and balanced charge carrier mobilities, and optimal morphology.

3. Conclusion

In summary, we described a feasible way to increase the performance of a BDT-alt-heteroacene-based highly scalable molecular design by introducing 2,5-difluoro benzene (2FBn) as a weak electron-acceptor core to form new WBG-PD, PBDT-2FBnT. The 2FBn is easily accessible at low-cost, and its corresponding monomer 2FBnT having two adjacent thiophene units is synthesized by a straightforward two-step process with > 82% yields. With the benefits of introducing a 2FBnT unit, PBDT-2FBnT showed a stronger absorption co-efficient of 5.39×10^4 M^{-1} cm^{-1}, deep HOMO energy levels (−5.48 eV), and strong aggregation leading to the increased crystallinity. Moreover, its optimal blend with ITIC also displayed well-matched energy levels with lower ΔE_{HOMO} offset, favorable face-on molecular orientation, high and well-balanced charge carrier mobilities, and favorable nanoscale morphology, so that corresponding NF-PSCs displayed a remarkable PCE of 9.5% with a superior trade-off between *V*oc of 0.919 V, and *J*sc of 16.1 mA/cm^2 was achieved. As a result, we believe that our detailed study on an easily scalable unit PBDT-2FBnT will encourage further explorations of easily scalable molecular designs that have tremendous potentials in commercial applications.

Declaration of Competing Interest

The authors declare that they have no known competing financial interests or personal relationships that could have appeared to influence the work reported in this paper.

Acknowledgements

This research was supported by the New & Renewable Energy Core Technology Program (No. 20193091010110) and Human Resources program in Energy Technology (No. 20194010201790) of the Korean Institute of Energy Technology Evaluation and Planning (KETEP) grant funded by the Ministry of Trade, Industry & Energy, Republic of Korea. This research was supported by the 2020 KU Brain Pool of Konkuk University.

Appendix A. Supplementary material

Supplementary data to this article can be found online at https://doi.org/10.1016/j.solener.2020.06.090.

References

Bai, H., Wu, Y., Wang, Y., Wu, Y., Li, R., Cheng, P., Zhang, M., Wang, J., Ma, W., Zhan, X., 2015. Nonfullerene acceptors based on extended fused rings flanked with benzothiadiazolylmethylenemalononitrile for polymer solar cells. J. Mater. Chem. A 3 (41), 20758–20766.

Berny, S., Blouin, N., Distler, A., Egelhaaf, H.-J., Krompiec, M., Lohr, A., Lozman, O.R., Morse, G.E., Nanson, L., Pron, A., Sauermann, T., Seidler, N., Tierney, S., Tiwana, P., Wagner, M., Wilson, H., 2016. Solar Trees: First large-scale demonstration of fully solution coated, semitransparent, flexible organic photovoltaic modules. Adv. Sci. 3 (5), 1500342.

Biniek, L., Fall, S., Chochos, C.L., Anokhin, D.V., Ivanov, D.A., Leclerc, N., Lévêque, P., Heiser, T., 2010. Impact of the alkyl side chains on the optoelectronic properties of a series of photovoltaic low-band-gap copolymers. Macromolecules 43 (23), 9779–9786.

Chen, S., Yao, H., Li, Z., Awartani, O.M., Liu, Y., Wang, Z., Yang, G., Zhang, J., Ade, H., Yan, H., 2017. Surprising effects upon inserting benzene units into a quaterthiophene-based D-A polymer-improving non-fullerene organic solar cells via donor polymer design. Adv. Energy Mater. 7 (12), 1602304.

Cui, Y., Yao, H., Hong, L., Zhang, T., Tang, Y., Lin, B., Xian, K., Gao, B., An, C., Bi, P., Ma, W., Hou, J., 2019a. 17% efficiency organic photovoltaic cell with superior processability. Natl. Sci. Rev. nwz200. https://doi.org/10.1093/nsr/nwz200.

Cui, Y., Yao, H., Hong, L., Zhang, T., Xu, Y., Xian, K., Gao, B., Qin, J., Zhang, J., Wei, Z., Hou, J., 2019b. Achieving over 15% efficiency in organic photovoltaic cells via copolymer design. Adv. Mater. 31 (14), 1808356.

Cui, Y., Yao, H., Zhang, J., Zhang, T., Wang, Y., Hong, L., Xian, K., Xu, B., Zhang, S., Peng, J., Wei, Z., Gao, F., Hou, J., 2019c. Over 16% efficiency organic photovoltaic cells enabled by a chlorinated acceptor with increased open-circuit voltages. Nat. Commun. 10 (1), 2515.

Dey, S., 2019. Recent progress in molecular design of fused ring electron acceptors for organic solar cells. Small 15 (21), 1900134.

Firdaus, Y., Maffei, L.P., Cruciani, F., Müller, M.A., Liu, S., Lopatin, S., Wehbe, N., Ndjawa, G.O.N., Amassian, A., Laquai, F., Beaujuge, P.M., 2017. Polymer main-chain substitution effects on the efficiency of nonfullerene BHJ solar cells. Adv. Energy Mater. 7 (21), 1700834.

Gao, Y., Zhu, R., Wang, Z., Guo, F., Wei, Z., Yang, Y., Zhao, L., Zhang, Y., 2018. An asymmetrical polymer based on thieno[2,3-f]benzofuran for efficient fullerene-free polymer solar cells. Adv. Energy Mater. 1 (5), 1888–1892.

Hadmojo, W.T., Wibowo, F.T.A., Lee, W., Jang, H.-K., Kim, Y., Sinaga, S., Park, M., Ju, S.-Y., Ryu, D.Y., Jung, I.H., Jang, S.-Y., 2019. Performance optimization of parallel-like ternary organic solar cells through simultaneous improvement in charge generation and transport. Adv. Funct. Mater. 29 (14), 1808731.

Hoefler, S.F., Rath, T., Pastukhova, N., Pavlica, E., Scheunemann, D., Wilken, S., Kunert, B., Resel, R., Hobisch, M., Xiao, S., Bratina, G., Trimmel, G., 2018. The effect of polymer molecular weight on the performance of PTB7-Th:O-IDTBR non-fullerene organic solar cells. J. Mater. Chem. A 6 (20), 9506–9516.

Holliday, S., Ashraf, R.S., Wadsworth, A., Baran, D., Yousaf, S.A., Nielsen, C.B., Tan, C.-H., Dimitrov, S.D., Shang, Z., Gasparini, N., Alamoudi, M., Laquai, F., Brabec, C.J., Salleo, A., Durrant, J.R., McCulloch, I., 2016. High-efficiency and air-stable P3HT-based polymer solar cells with a new non-fullerene acceptor. Nat. Commun. 7 (1), 11585.

Hong, L., Yao, H., Wu, Z., Cui, Y., Zhang, T., Xu, Y., Yu, R., Liao, Q., Gao, B., Xian, K., Woo, H.Y., Ge, Z., Hou, J., 2019. Eco-compatible solvent-processed organic photovoltaic cells with over 16% efficiency. Adv. Mater. 1903441.

Jeon, S.J., Han, Y.W., Moon, D.K., 2019a. Chlorine effects of heterocyclic ring-based donor polymer for low-cost and high-performance nonfullerene polymer solar cells. Sol. RRL 3 (7), 1900094.

Jeon, S.J., Han, Y.W., Moon, D.K., 2019b. Drastic changes in properties of donor-acceptor polymers induced by asymmetric structural isomers for application to polymer solar cells. ACS Appl. Mater. Interfaces 11 (9), 9239–9250.

Kini, G.P., Choi, J.Y., Jeon, S.J., Suh, I.S., Moon, D.K., 2018. Controlling the interchain packing and photovoltaic properties via fluorine substitution in terpolymers based on benzo[1,2-c:4,5-c']dithiophene-4,8-dione and benzothiadiazole units. Polymer 148, 330–338.

Kini, G.P., Choi, J.Y., Jeon, S.J., Suh, I.S., Moon, D.K., 2019. Effects of incorporated pyrazine on the interchain packing and photovoltaic properties of wide-bandgap D-A polymers for non-fullerene polymer solar cells. Polym. Chem. 10 (32), 4459–4468.

Kini, G.P., Hoang, Q.V., Song, C.E., Lee, S.K., Shin, W.S., So, W.-W., Uddin, M.A., Woo, H.Y., Lee, J.-C., 2017a. Thiophene-benzothiadiazole based D-A1–D–A2 type alternating copolymers for polymer solar cells. Polym. Chem. 8 (23), 3622–3631.

Kini, G.P., Jeon, S.J., Moon, D.K., 2020. Design principles and synergistic effects of chlorination on a conjugated backbone for efficient organic photovoltaics: a critical review. Adv. Mater. 32 (11), 1906175.

Kini, G.P., Lee, S.K., Shin, W.S., Moon, S.-J., Song, C.E., Lee, J.-C., 2016. Achieving a solar power conversion efficiency exceeding 9% by modifying the structure of a simple, inexpensive and highly scalable polymer. J. Mater. Chem. A 4 (47), 18585–18597.

Kini, G.P., Oh, S., Abbas, Z., Rasool, S., Jahandar, M., Song, C.E., Lee, S.K., Shin, W.S., So, W.-W., Lee, J.-C., 2017b. Effects on photovoltaic performance of dialkyloxy-benzothiadiazole copolymers by varying the thienoacene donor. ACS Appl. Mater. Interfaces 9 (14), 12617–12628.

Li, C., Yue, Q., Wu, H., Li, B., Fan, H., Zhu, X., 2021. Small bandgap non-fullerene acceptor enables efficient PTB7-Th solar cell with near 0 eV HOMO offset. J. Energy Chem. 52, 60–66.

Li, L., Feng, L., Yuan, J., Peng, H., Zou, Y., Li, Y., 2018a. Fine-tuning blend morphology via alkylthio side chain engineering towards high performance non-fullerene polymer solar cells. Chem. Phys. Lett. 696, 19–25.

Li, S., Ye, L., Zhao, W., Yan, H., Yang, B., Liu, D., Li, W., Ade, H., Hou, J., 2018b. A wide band gap polymer with a deep highest occupied molecular orbital level enables 14.2% efficiency in polymer solar cells. J. Am. Chem. Soc. 140 (23), 7159–7167.

Li, X., Huang, H., Bin, H., Peng, Z., Zhu, C., Xue, L., Zhang, Z.-G., Zhang, Z., Ade, H., Li, Y., 2017a. Synthesis and photovoltaic properties of a series of narrow bandgap organic semiconductor acceptors with their absorption edge reaching 900 nm. Chem. Mater. 29 (23), 10130–10138.

Li, Y., Lin, J.D., Che, X., Qu, Y., Liu, F., Liao, L.S., Forrest, S.R., 2017b. High efficiency near-infrared and semitransparent non-fullerene acceptor organic photovoltaic cells. J. Am. Chem. Soc. 139 (47), 17114–17119.

Li, Y., Xu, G., Cui, C., Li, Y., 2018c. Flexible and semitransparent organic solar cells. Adv. Energy Mater. 8 (7), 1701791.
Liao, Z., Xie, Y., Chen, L., Tan, Y., Huang, S., An, Y., Ryu, H.S., Meng, X., Liao, X., Huang, B., Xie, Q., Woo, H.Y., Sun, Y., Chen, Y., 2019. Fluorobenzotriazole (FTAZ)-based polymer donor enables organic solar cells exceeding 12% efficiency. Adv. Funct. Mater. 29 (10), 1808828.
Lin, F., Huang, W., Sun, H., Xin, J., Zeng, H., Yang, T., Li, M., Zhang, X., Ma, W., Liang, Y., 2017. Thieno[3,4-c]pyrrole-4,6(5H)-dione polymers with optimized energy level alignments for fused-ring electron acceptor based polymer solar cells. Chem. Mater. 29 (13), 5636–5645.
Lin, Y., Wang, J., Zhang, Z.-G., Bai, H., Li, Y., Zhu, D., Zhan, X., 2015. An electron acceptor challenging fullerenes for efficient polymer solar cells. Adv. Mater. 27 (7), 1170–1174.
Liu, H., Li, Z.a., Zhao, D., 2019. Rhodanine-based nonfullerene acceptors for organic solar cells. Sci. China Mater. 62 (11), 1574–1596.
Liu, T., Luo, Z., Chen, Y., Yang, T., Xiao, Y., Zhang, G., Ma, R., Lu, X., Zhan, C., Zhang, M., Yang, C., Li, Y., Yao, J., Yan, H., 2019. A nonfullerene acceptor with a 1000 nm absorption edge enables ternary organic solar cells with improved optical and morphological properties and efficiencies over 15%. Energy Environ. Sci. 12 (8), 2529–2536.
Lu, L., Zheng, T., Wu, Q., Schneider, A.M., Zhao, D., Yu, L., 2015. Recent advances in bulk heterojunction polymer solar cells. Chem. Rev. 115 (23), 12666–12731.
Luo, M., Zhu, C., Yuan, J., Zhou, L., Keshtov, M.L., Godovsky, D.Y., Zou, Y., 2019. A chlorinated non-fullerene acceptor for efficient polymer solar cells. Chin. Chem. Lett. 30 (12), 2343–2346.
Ma, Y., Kang, Z., Zheng, Q., 2017. Recent advances in wide bandgap semiconducting polymers for polymer solar cells. J. Mater. Chem. A 5 (5), 1860–1872.
Pai, R.K., Ahipa, T.N., Hemavathi, B., 2016. Rational design of benzodithiophene based conjugated polymers for better solar cell performance. RSC Adv. 6 (28), 23760–23774.
Park, G.E., Choi, S., Park, S.Y., Lee, D.H., Cho, M.J., Choi, D.H., 2017. Eco-friendly solvent-processed fullerene-free polymer solar cells with over 9.7% efficiency and long-term performance stability. Adv. Energy Mater. 7 (19), 1700566.
Sharma, R., Lee, H., Seifrid, M., Gupta, V., Bazan, G.C., Yoo, S., 2020. Performance enhancement of conjugated polymer-small molecule-non fullerene ternary organic solar cells by tuning recombination kinetics and molecular ordering. Sol. Energy 201, 499–507.
Song, X., Gasparini, N., Baran, D., 2018. The influence of solvent additive on polymer solar cells employing fullerene and non-fullerene acceptors. Adv. Electron. Mater. 4 (10), 1700358.
Strohm, S., Machui, F., Langner, S., Kubis, P., Gasparini, N., Salvador, M., McCulloch, I., Egelhaaf, H.J., Brabec, C.J., 2018. P3HT: non-fullerene acceptor based large area, semi-transparent PV modules with power conversion efficiencies of 5%, processed by industrially scalable methods. Energy Environ. Sci. 11 (8), 2225–2234.
Su, W., Li, G., Fan, Q., Zhu, Q., Guo, X., Chen, J., Wu, J., Ma, W., Zhang, M., Li, Y., 2019. Nonhalogen solvent-processed polymer solar cells based on chlorine and trialkylsilyl substituted conjugated polymers achieve 12.8% efficiency. J. Mater. Chem. A 7 (5), 2351–2359.
Wadsworth, A., Moser, M., Marks, A., Little, M.S., Gasparini, N., Brabec, C.J., Baran, D., McCulloch, I., 2019. Critical review of the molecular design progress in non-fullerene electron acceptors towards commercially viable organic solar cells. Chem. Soc. Rev. 48 (6), 1596–1625.
Wang, T., Sun, R., Xu, S., Guo, J., Wang, W., Guo, J., Jiao, X., Wang, J., Jia, S., Zhu, X., Li, Y., Min, J., 2019. A wide-bandgap D-A copolymer donor based on a chlorine substituted acceptor unit for high performance polymer solar cells. J. Mater. Chem. A 7 (23), 14070–14078.
Wienhold, K.S., Körstgens, V., Grott, S., Jiang, X., Schwartzkopf, M., Roth, S.V., Müller-Buschbaum, P., 2019. Effect of solvent additives on the morphology and device performance of printed nonfullerene acceptor based organic solar cells. ACS Appl. Mater. Interfaces 11 (45), 42313–42321.
Wu, Y., Yang, H., Zou, Y., Dong, Y., Yuan, J., Cui, C., Li, Y., 2019. A new dialkylthio-substituted naphtho[2,3-c]thiophene-4,9-dione based polymer donor for high-performance polymer solar cells. Energy Environ. Sci. 12 (2), 675–683.
Xu, S., Wang, X., Feng, L., He, Z., Peng, H., Cimrová, V., Yuan, J., Zhang, Z.-G., Li, Y., Zou, Y., 2018. Optimizing the conjugated side chains of quinoxaline based polymers for nonfullerene solar cells with 10.5% efficiency. J. Mater. Chem. A 6 (7), 3074–3083.
Yang, F., Li, C., Lai, W., Zhang, A., Huang, H., Li, W., 2017. Halogenated conjugated molecules for ambipolar field-effect transistors and non-fullerene organic solar cells. Mater. Chem. Front. 1 (7), 1389–1395.
Yang, J., Uddin, M.A., Tang, Y., Wang, Y., Wang, Y., Su, H., Gao, R., Chen, Z.-K., Dai, J., Woo, H.Y., Guo, X., 2018. Quinoxaline-based wide band gap polymers for efficient nonfullerene organic solar cells with large open-circuit voltages. ACS Appl. Mater. Interfaces 10 (27), 23235–23246.
Ye, L., Zhang, S., Huo, L., Zhang, M., Hou, J., 2014. Molecular design toward highly efficient photovoltaic polymers based on two-dimensional conjugated benzodithiophene. Acc. Chem. Res. 47 (5), 1595–1603.
Yuan, J., Zhang, Y., Zhou, L., Zhang, C., Lau, T.-K., Zhang, G., Lu, X., Yip, H.-L., So, S.K., Beaupré, S., Mainville, M., Johnson, P.A., Leclerc, M., Chen, H., Peng, H., Li, Y., Zou, Y., 2019a. Fused benzothiadiazole: a building block for n-type organic acceptor to achieve high-performance organic solar cells. Adv. Mater. 31 (17), 1807577.
Yuan, J., Zhang, Y., Zhou, L., Zhang, G., Yip, H.-L., Lau, T.-K., Lu, X., Zhu, C., Peng, H., Johnson, P.A., Leclerc, M., Cao, Y., Ulanski, J., Li, Y., Zou, Y., 2019b. Single-junction organic solar cell with over 15% efficiency using fused-ring acceptor with electron-deficient core. Joule 3 (4), 1140–1151.
Zhang, J., Li, Y., Hu, H., Zhang, G., Ade, H., Yan, H., 2019. Chlorinated thiophene end groups for highly crystalline alkylated non-fullerene acceptors toward efficient organic solar cells. Chem. Mater. 31 (17), 6672.
Zhang, Q., Kelly, M.A., Bauer, N., You, W., 2017a. The curious case of fluorination of conjugated polymers for solar cells. Acc. Chem. Res. 50 (9), 2401–2409.
Zhang, S., Qin, Y., Zhu, J., Hou, J., 2018a. Over 14% efficiency in polymer solar cells enabled by a chlorinated polymer donor. Adv. Mater. 30 (20), 1800868.
Zhang, Y., Yao, H., Zhang, S., Qin, Y., Zhang, J., Yang, L., Li, W., Wei, Z., Gao, F., Hou, J., 2018b. Fluorination vs. chlorination: a case study on high performance organic photovoltaic materials. Sci. China Chem. 61 (10), 1328–1337.
Zhang, Z., Liu, W., Rehman, T., Ju, H.-X., Mai, J., Lu, X., Shi, M., Zhu, J., Li, C.-Z., Chen, H., 2017b. Energy-level modulation of non-fullerene acceptors to achieve high-efficiency polymer solar cells at a diminished energy offset. J. Mater. Chem. A 5 (20), 9649–9654.
Zhao, W., Li, S., Yao, H., Zhang, S., Zhang, Y., Yang, B., Hou, J., 2017. Molecular optimization enables over 13% efficiency in organic solar cells. J. Am. Chem. Soc. 139 (21), 7148–7151.